Plasmon-Assisted Degradation of Toxic Pollutants with Ag−AgBr/Al_2O_3 under Visible-Light Irradiation

Xuefeng Zhou, Chun Hu,* Xuexiang Hu, Tianwei Peng, and Jiuhui Qu

State Key Laboratory of Environmental Aquatic Chemistry, Research Center for Eco-Environmental Sciences, Chinese Academy of Sciences, Beijing, 100085, China

Received: October 9, 2009; Revised Manuscript Received: December 14, 2009

AgBr coated with silver (Ag) nanoparticles (NPs) were highly dispersed on ordered mesoporous γ-Al_2O_3 (MA) by the deposition−precipitation method with surfactant (Ag−AgBr/MAP). The catalyst showed high and stable photocatalytic activity for the degradation and mineralization of toxic persistent organic pollutants, as demonstrated with 2-chlorophenol (2-CP), 2,4-dichlorophenol, and trichlorophenol under visible light or simulated solar light irradiation. The dispersion of Ag−AgBr NPs on MA strongly affected their photoactivity. On the basis of electron spin resonance and cyclic voltammetry analyses under a variety of experimental conditions, two plasmon-induced electron-transfer processes were verified from the excited Ag NPs to AgBr and from 2-CP to the Ag NPs, resulting in $O_2^{\bullet-}$ and excited h^+ on Ag NPs. Also, $^{\bullet}OH$ and $O_2^{\bullet-}$ were formed by photoexcited AgBr. Both $^{\bullet}OH$ and $O_2^{\bullet-}$ radicals were primary active species, whereas the excited h^+ on Ag NPs was involved in the photoreaction system of Ag−AgBr/MAP. The highly efficient degradation of pollutants came from both photoexcited AgBr and plasmon-excited Ag NPs. Accordingly, the plasmon-induced electron-transfer processes elucidated the photostability of Ag−AgBr/MAP. These findings indicate potential applications of noble metal NPs in the fields of developing visible-light-sensitive photocatalysts and photovoltaic fuel cells.

Introduction

Heterogeneous photocatalysis has been considered as cost-effective alternative for the destruction of persistent toxic organic compounds.[1,2] One obstacle to its practical application is the inefficient use of solar energy. The development of visible-light photocatalysts has become one of the most important topics in the photocatalysis field. There are two approaches to exploit the photocatalysts responsive to visible light: the first involved the substitutional doping of metals and nonmetals for some UV-active oxide, such as TiO_2[3−6] and $InTaO_4$[7] to turn visible photocatalysts. The second is the composite metal oxides visible photocatalysts, such as $PbBi_2Nb_2O_9$,[8] Bi_2WO_6,[9] and $CaFe_2O_4$/$PbBi_2Nb_{1.9}W_{0.1}O_9$.[10] However, these photocatalysts still could not be applied for the practical solar purification due to low activity and stability. New and more efficient visible-light photocatalysts are needed to meet the requirements of future environmental and energy technologies driven by solar energy.

Noble metal nanoparticles (NPs) exhibit strong UV−vis absorption due to their plasmon resonance, which is produced by the collective oscillations of surface electrons.[11,12] In particular, Ag NPs show efficient plasmon resonance in the visible region, which has been investigated in contact with different semiconductors.[13−18] When Ag NPs were in direct contact with TiO_2, it did not enhance the catalytic activity but showed a negative effect due to the oxidation of Ag NPs. Oppositely, when Ag NPs coated with SiO_2 were supported on TiO_2, the photocatalytic activity was greatly enhanced. In the other cases, Ag^0 NPs existed stably on the surface of AgBr/TiO_2[19] and AgBr/$WO_3\cdot H_2O$,[20] which exhibited high activity and stability for the destruction of the pollution under visible light. However, the plasmon-induced photocatalytic mechanism and the stability of noble metallic NPs during the photocatalytic degradation have not, to our knowledge, been reported.

The plasmon-induced activity of noble metal NPs depends on the size distribution and morphology of particles, which are affected primarily by the preparation method, the nature of the support. Presently, using porous materials as solid nanoreactors, different nanocrystals with various morphologies have been obtained by a method called "nanocasting".[21] Generally, inorganic precursors are first introduced into channels of host materials such as mesoporous silicas. Then, nanocrystals are produced with a replica of the confined space by subsequent reaction. Ordered mesoporous materials, with their intrinsically high surface areas, are particularly suitable for this purpose. Mesoporous alumina has been widespread and used as catalyst supports, and its physical properties such as surface area, pore distribution, and volume have significant effect on its performance in application.

In this paper, Ag−AgBr NPs were highly dispersed on the surface and channels of synthetic ordered mesoporous γ-Al_2O_3 (MA) by the deposition−precipitation method under different conditions. Several ubiquitous water pollutants 2-chlorophenol (2-CP), 2,4-dichlorophenol (2,4-DCP), and trichlorophenol (TCP) were selected to evaluate the activity and properties of the catalyst under visible light irradiation. Ag−AgBr/MAP exhibited much higher reactivity for these tested pollutants, which came from the photoexcited AgBr and plasmon-induced Ag NPs. The dispersion and size of Ag−AgBr NPs strongly affected the photoactivity. A plasmon-induced photocatalytic mechanism was verified by electron spin resonance (ESR) and cyclic voltammetry analyses (CV) under a variety of experimental conditions. Our findings suggest that the high photosensitivity of noble metal NPs due to surface plasmon resonance could be applied toward the development of new plasmonic visible-light-sensitive photocatalysts and photovoltaic fuel cells.

* Corresponding author. Tel: +86-10-62849628. Fax: +86-10-62923541; E-mail: huchun@rcees.ac.cn.

10.1021/jp909697k
Published on Web 01/22/2010

Experimental Section

Chemicals and Materials. The reagent 5,5-dimethyl-1-pyrroline *N*-oxide (DMPO), used as the spin trapping agent in the ESR studies, was purchased from the Sigma Chemical Co. All other chemicals used were analytical grade, purchased from Beijing Chemical Co. and used without further purification.

Catalyst Preparation. Mesoporous γ-Al_2O_3 (MA) was prepared from precursors of aluminum isopropoxide in the presence of glucose in an aqueous system as described previously.[22,23] Ag−AgBr was deposited onto MA using a deposition-precipitation method. Briefly, a 0.6 g quantity of MA was added to 60 mL of distilled water, and the suspension was sonicated for 30 min. Then, 1.3 g of NaBr was added to the suspension, and the mixture was stirred magnetically for 30 min, and then sonicated for 30 min. Subsequently, 0.6 g poly(ethylene glycol)-*block*-poly(ethylene glycol) (P123) was added to the suspension, and the mixture was stirred magnetically for 30 min and then sonicated for 30 min. Then, 1.3 g of $AgNO_3$ in 1.8 mL of NH_4OH (25 wt % NH_3) was quickly added to the mixture. In this process, at alkaline condition, cationic surfactant P123 could adsorb onto the surface of MA to limit the number of nucleation sites for a AgBr metal island to grow, leading to uniformly dispersed AgBr. The resulting suspensions were stirred at room temperature for 12 h. All the above processes were carried out in a dark situation. Then, the amount of Ag^+ in the supernatant was measured by inductively coupled plasma optical emission spectrometry (ICP-OES) on an OPTIMA 2000 (Perkin-Elmer Co.) instrument, confirming that the Ag content of 10 wt % was incorporated in MA. The product was filtered, washed with water, and dried at 70 °C. Finally, the powder was calcined in air at 500 °C for 3 h. The prepared photocatalyst was designated by Ag−AgBr/MAP. As reference, Ag−AgBr/MA with 10 wt % Ag content was also prepared without the addition of surfactant P123 according to the same procedure. Meanwhile, Ag/Al_2O_3 was prepared by incipient wetness impregnation. A 0.052 g amount of $AgNO_3$ was dissolved in a volume of deionized water equal to that of the porous volume of 0.6 g of Al_2O_3. The solutions were then deposited on the Al_2O_3 by the incipient wetness impregnation method at room temperature. The samples were dried at 120 °C for 2 h, calcined in air at 600 °C for 6 h, and then reduced in a stream of H_2/N_2 (20 vol % H_2, 50 mL min^{-1}) at 400 °C for 2 h.

Characterization. The samples were examined by obtaining X-ray diffraction (XRD) patterns (XDS-2000 diffractometer; Scintag Inc., Sunnyvale, CA) and UV−vis diffuse reflectance spectra (Hitachi UV-3100). The high-resolution transmission electron microscopy (HRTEM) images associated with energy-dispersive X-ray spectroscopy (EDX) analyses were performed by using a JEOL-2010 TEM with an acceleration voltage of 200 kV. ESR spectra were obtained using a Bruker model ESP 300 E electron paramagnetic resonance spectrometer equipped with a Quanta-Ray Nd:YAG laser system as the irradiation source ($\lambda = 532$ nm). The photocurrent from the various samples was measured in a basic electrochemical system (AMETEK Princeton Applied Research, Oak Ridge, TN) with a two-compartment, three-electrode electrochemical cell equipped with a photocatalyst photoanode (prepared by dip-coating and drying in air at 70 °C) and a platinum wire cathode in a 0.1 M Na_2SO_4 solution. The reference electrode was a saturated calomel electrode.

Photocatalytic Degradation of Chlorophenolic Compounds under Visible Light. Photocatalytic experiments were performed in a beaker with aqueous suspensions of chlorophenol (60 mL, 10 mg L^{-1}) and 100 mg of catalyst powder. The light source was a 350 W Xe-arc lamp (Shanghai Photoelectron Device Ltd.) equipped with wavelength cutoff filters for $\lambda >$ 420 and focused onto the beaker. The concentration of each chlorophenol was measured using high-performance liquid chromatography (1200 series; Agilent, Santa Clara, CA) with an Eclipse XDB-C18 column (5 μm, 4.6 × 150 mm; Agilent). The total organic carbon (TOC) of each solution was measured with an Apollo 9000 TOC analyzer (Teledyne Tekmar, Mason, OH).

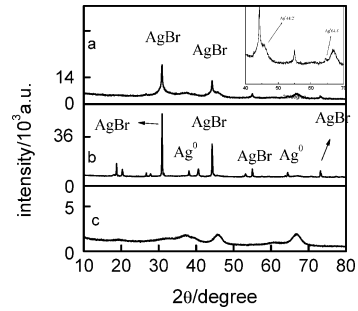

Figure 1. XRD pattern of (a) Ag−AgBr/MAP, (b) Ag−AgBr/MA, and (c) MA. Inset: XRD peaks of Ag^0 in Ag−AgBr/MAP.

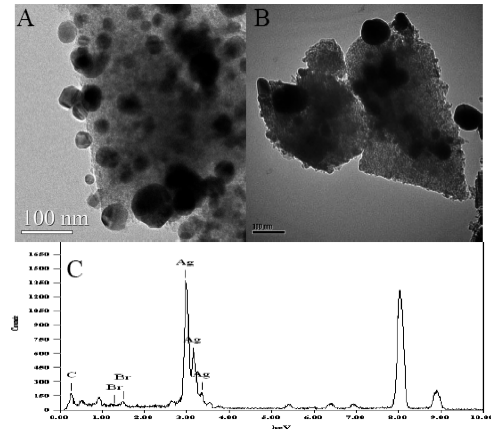

Figure 2. Representative HRTEM image of (A) Ag−AgBr/MAP and (B) Ag−AgBr/MA. (C) Corresponding EDX pattern of Ag−AgBr/MAP.

Results and Discussion

Characterization of Catalysts. Figure 1 shows the XRD pattern of the different samples. The coexistence of Ag (JCPDS 65−2871) and AgBr (JCPDS 06-0438) was observed in both Ag−AgBr/MAP and Ag−AgBr/MA. However, the intensities of the XRD diffraction peaks of the former were much lower than those of the latter, indicating the smaller crystallite size of Ag−AgBr in Ag−AgBr/MAP. Figure 2A,B shows HRTEM images of the both samples. Obviously, Ag−AgBr NPs were uniformly highly dispersed on the surface of MA for Ag−AgBr/MAP. Their crystalline sizes were in the range 20−50 nm, and the shape was a regular cubic structure. Oppositely, Ag−AgBr NPs were aggregated and the crystalline size was more than 100 nm in Ag−AgBr/MA. The results were in agreement with that of XRD. Figure 2C shows the EDX spectrum of Ag−AgBr NPs in Ag−AgBr/MAP. Only silver and bromine were observed (copper and carbon signals arose from the TEM grid). The ratio of Ag:Br atoms is approximately 55.79:1.89, indicating that AgBr NPs were covered with Ag NPs. The diffuse reflectance UV−vis spectra of Ag−AgBr/MAP, Ag−AgBr/MA, and N-doped TiO_2 ($TiO_{2-x}N_x$) as a reference photocatalyst are compared in Figure 3. Ag−AgBr/MAP has a much stronger UV

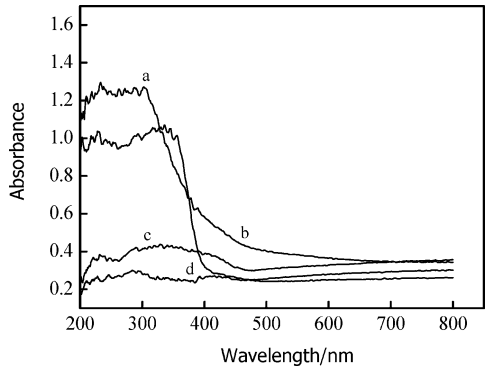

Figure 3. UV−vis diffuse reflectance spectra of (a) Ag−AgBr/MAP, (b) $TiO_{2-x}N_x$, (c) Ag−AgBr/MA, and (d) MA.

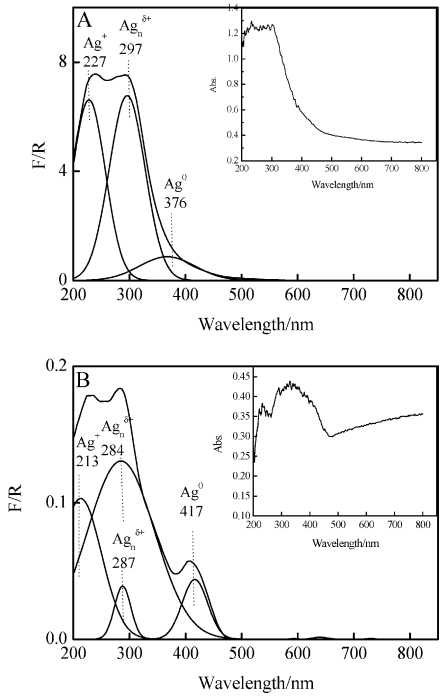

Figure 4. Deconvoluted subbands of Ag−AgBr/MAP (A) and Ag−AgBr/MA (B). Inset: relative UV−vis absorption spectra of Ag−AgBr/MAP (A) and Ag−AgBr/MA (B).

absorption than Ag−AgBr/MA, indicating that the former has the smaller size of Ag−AgBr NPs. The both catalysts also exhibit a band around 400−700 nm in visible region assigned to the mixed peaks from the plasmon resonance of Ag NPs and light absorption of AgBr. Furthermore, the relative UV−vis absorption spectra of Ag−AgBr was the difference spectra between those of the supported Ag−AgBr and MA (Figure 4). The bands at 227 and 213 nm were attributed to the highly dispersed Ag^+ ions,[22] the bands at 284 and 297 nm were assigned to small $Ag_n^{\delta+}$ clusters from AgBr.[24] The bands at 376 and 417 nm were attributed to Ag^0 NPs.[25] The other plasmon absorption bands at more than 450 nm were so weak that they were overlaid by MA baseline, which were observed in the following experiments. Subsequently, the spectra were converted into Kubelka−Munk functions and deconvoluted into Gaussian subbands that could be assigned to different Ag species.[26] The deconvolution was carried out on the basis of the relative intensities of these subbands, and the corresponding percentage of the different Ag species was obtained. Thus, in Ag−AgBr/MAP and Ag−AgBr/MA, the contents of Ag^0 species were 1.04 and 0.62 wt %, whereas the contents of dispersed Ag^+ ions were 3.81 and 2.25 wt %, and those of $Ag_n^{\delta+}$ clusters

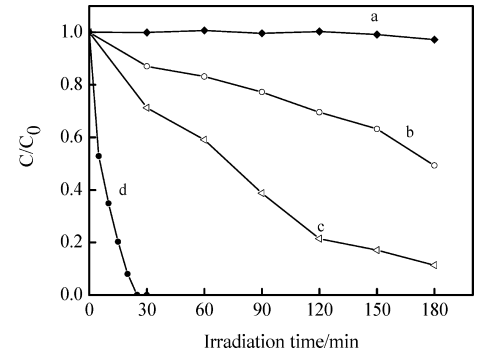

Figure 5. Temporal course of photodegradation of 2-CP (10 mg L^{-1}; 60 mL) in aqueous dispersions (containing catalyst: 1.6 g L^{-1}) under visible light irradiation ($\lambda > 420$ nm): (a) Ag−AgBr/MAP in dark and (b) $TiO_{2-x}N_x$, (c) Ag−AgBr/MA, and (d) Ag−AgBr/MAP.

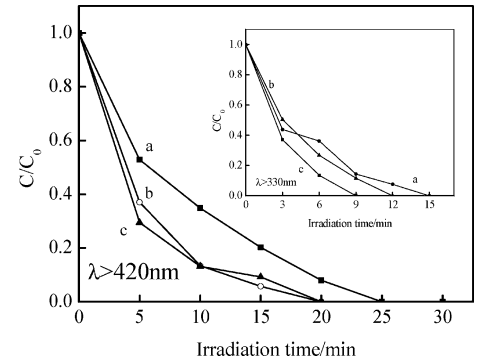

Figure 6. Photodegradation of different pollutants (10 mg L^{-1}) in aqueous dispersions of Ag−AgBr/MAP under visible light [$\lambda > 420$ nm and $\lambda > 330$ nm (inset)] simulated solar irradiation: (a) 2-CP; (b) 2,4-DCP; (c) TCP.

3.65 and 5.63 wt %, repectively. The results also indicated that Ag−AgBr NPs were more highly dispersed on MA in the presence of P123.

Photodegradation of Pollutants under Visible Light Irradiation. The photocatalytic activity of different catalysts was evaluated by the photodegradation of 2-chlorophenol (2-CP) under visible irradiation ($\lambda > 420$ nm). As shown in Figure 5, no significant degradation of 2-CP was observed in dark Ag−AgBr/MAP suspensions, while 2-CP was completely photodegraded within 25 min under visible light irradiation. Only 30% of 2-CP was degraded in Ag−AgBr/MA at the same time under otherwise identical conditions. The results indicated that the photocatalytic activity predominantly depended on the dispersion and crystalline size of Ag−AgBr NPs on the MA. Moreover, Ag−AgBr/MAP showed much greater activity than $TiO_{2-x}N_x$. In the Ag−AgBr/MAP suspension, about 80% of TOC was removed with the degradation of 2-CP after illumination for 120 min. By GC−MS analysis, the main intermediates were aliphatic acids and alcohol in the reaction solution. In addition, 2,4-DCP and TCP were completely degraded within 20 min, respectively, in Ag−AgBr/MAP suspension under visible light irradiation (Figure 6). TOC removals of 73% and 71% were obtained after 120 min for 2,4-DCP, and TCP, respectively (Figure 7). Furthermore, under $\lambda > 330$ nm irradiation of the Xe arc lamp, which produces light spectra similar to that of solar radiation, the tested compounds were completely degraded within 9−15 min, and around 80% of the TOC was removed after 60 min in Ag−AgBr/MAP suspension (Figure 7). The degradation rates of these initial compounds increased in the order 2-CP < 2,4-DCP < TCP, while their mineralization rates exhibited the opposite order. The sequences

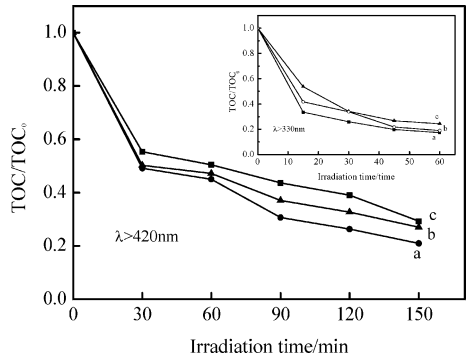

Figure 7. Removal of TOC for various pollutants (10 mg L^{-1}) in aqueous dispersions of Ag−AgBr/MAP under visible light [$\lambda > 420$ nm and $\lambda > 330$ nm (inset)] simulated solar irradiation: (a) 2-CP; (b) 2,4-DCP; (c) TCP.

were different between the degradation of initial compounds and their mineralization due to different oxidation reactions. The former mainly involved dechlorination, while the latter involved further degradation of byproducts. Some byproducts from 2,4-DCP and TCP still contained chlorine groups on the benzene ring, leading to the lower degradation rate. The photocatalytic activity did not decrease after five successive cycles of degradation testing under visible irradiation (Supporting Information Figure S1). These results indicate that Ag−AgBr/MAP is an effective and stable photocatalyst under solar light.

Reaction Mechanism. The ESR spin-trap technique (with DMPO) was used to detect the nature of the reactive oxygen species generated on the surface of catalysts under visible irradiation. A Nd: YAG laser ($\lambda = 532$ nm) was employed to irradiate suspensions containing catalysts. Four characteristic peaks of DMPO−$^{\bullet}$OH and six characteristic peaks of the DMPO−$O_2^{\bullet-}$ adducts were observed in Ag−AgBr/MAP suspension (Figure 8). No such signals were detected in dark. This means that irradiation is essential to the generation of $^{\bullet}$OH and $O_2^{\bullet-}$ on the surface of the catalyst. The effects of various radical scavengers, including the HCO_3^-, methanol, and *tert*-butanol scavengers of $^{\bullet}$OH radicals, and $O_2^{\bullet-}$ scavenger *p*-benzoquinone, on the degradation of 2-CP were examined. As shown in Figure 9, the degradation of 2-CP was markedly suppressed with the addition of *tert*-butanol within reaction 10 min, subsequently, the suppression decreased due to the degradation of *tert*-butanol, causing the complete removal of 2-CP at the same time as before. Also, methanol significantly depressed the degradation of 2-CP throughout the reaction, leading to 76% of 2-CP removal at 30 min, whereas the degradation of 2-CP was depressed to some extent in the presence of HCO_3^- ions. The addition of *p*-benzoquinone led to a greatest suppression in the photodegradation rate of degradation of 2-CP. Since methanol and *tert*-butanol hardly adsorbed on the catalyst, they predominantly scavenged $^{\bullet}$OH in solution. HCO_3^- was found to have high adsorption on the surface of the catalyst. The adsorbed HCO_3^- mainly reacted with h^+ and adsorbed $^{\bullet}$OH on the catalyst, leading to lower activity. Accordingly, these results suggested that both $^{\bullet}$OH and $O_2^{\bullet-}$ radicals in solution were the primary active species, while both h^+ and adsorbed $^{\bullet}$OH on the catalyst also were involved. Furthermore, the charge separation and charge-transfer processes on Ag−AgBr NPs were followed by CV analyses with visible light irradiation. The photocurrents of the photoanode were measured under different conditions. In a N_2-saturated 0.1 M sodium sulfate aqueous solution (Figure 10A), no significant photocurrent was detected at the Ag−AgBr/MAP photoanode in the dark. However, under visible irradiation, the photocurrent increased and then decreased to a stable value,

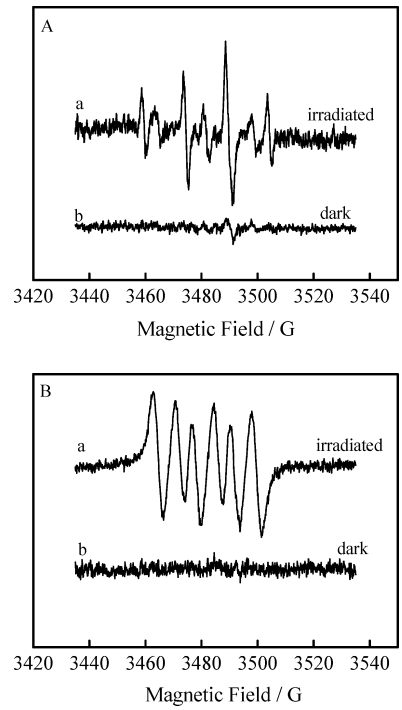

Figure 8. DMPO spin-trapping ESR spectra recorded at ambient temperature in aqueous dispersion for DMPO−$^{\bullet}$OH (A) and methanol dispersion for DMPO−$O_2^{\bullet-}$ (B) under visible light irradiation (532 nm): (a) Ag−AgBr/MAP; (b) Ag−AgBr/MAP in dark.

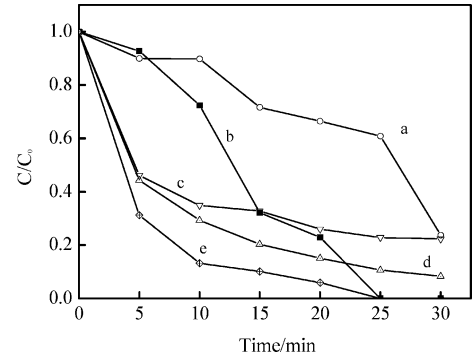

Figure 9. Plotted degradation kinetics of 2-CP in Ag−AgBr/MAP suspension (1.6 g L^{-1}) under visible irradiation ($\lambda > 420$ nm) with (a) 0.1 mM *p*-benzoquinone, (b) *tert*-butanol, (c) $NaHCO_3$, (d) methanol, and (e) no scavenger added. Scavenger concentration: 0.1 M.

resulting in a peak. The intensity of this peak decreased as the illumination wavelength was increased from 420 to 600 nm, which was assigned to the oxidation of Ag NPs due to the plasmon-excited charge separation. After the oxidation of Ag NPs, the photocurrents still were not zero, coming from photoexcited AgBr. With the addition of Fe^{2+} ions to act as electron donors, the peaks gradually decreased, becoming indiscernible at 1 mM Fe^{2+}, with the consequent formation of a stable photocurrent more than that before. In the Ag−AgBr/MAP system, photocurrent generation was ascribed to the plasmon-excited Ag NPs and photoexcited AgBr, indicating that the photoactivity of Ag−AgBr/MAP was contributed to the plasmon resonance of Ag NPs and photoexcited AgBr. In addition, neither oxidation of Ag nor photocurrent was observed at the Ag/Al_2O_3 photoanode under the otherwise identical conditions (Supporting Information Figure S2). It was confirmed that plasmon-induced electron transfer did not occur from Ag NPs to Al_2O_3 although Ag/Al_2O_3 had plasmon resonance in visible region (Supporting Information Figure S3). The results

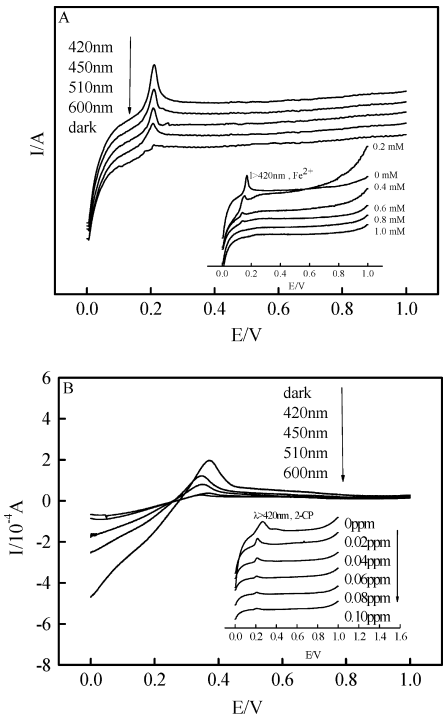

Figure 10. Photocurrent changes at the photoanode in N_2-saturated (A) and air-saturated (B) 0.1 M sodium sulfate aqueous solutions under the specified conditions.

indicated that an electron from the plasmon-excited Ag NPs transferred to the conduction band of AgBr at visible light-irradiated Ag−AgBr/MAP photoanode. A similar phenomenon was observed in air at the Ag−AgBr/MAP photoanode (Figure 10B). Differently, the oxidation peak of Ag NPs was observed even in the dark due to the presence of oxygen. However, Ag NPs were not oxidized at Ag/Al_2O_3 in air due to the passive support (Supporting Information Figure S4). With the addition of 2-CP, the photocurrent dropped to zero and the oxidation peak disappeared. This result revealed that 2-CP could be oxidized by plasmon-induced h^+ on Ag NPs, thereby accelerating the photooxidized Ag NPs back to their initial state. This confirmed that plasmon-induced h^+ on Ag NPs was also an active species. The $O_2^{\bullet-}$ radicals were generated by O_2 trapping the electron in the conduction band (CB) of AgBr coming from both photoexcited AgBr and plasmon-photoexcited Ag NPs. The oxidation of 2-CP consumed $O_2^{\bullet-}$ quenching any photocurrent. On the basis of all the information, for the plasmon-induced electron, two electron-transfer processes occurred during the degradation of 2-CP. One electron transfer occurred from the plasmon-photoexcited Ag NPs to the CB of AgBr, resulting in the formation of $O_2^{\bullet-}$. The other electron transfer occurred from 2-CP to the Ag NPs. Due to the plasmon-induced charge separation and transfer, Ag NPs were not corrupted by light and resulted in significantly more stable Ag halides. In addition, it also was verified that $^{\bullet}OH$ and $O_2^{\bullet-}$ are produced from visible photoexcited AgBr in Ag−AgBr/MAP creating electron−hole pairs to react with adsorbed oxygen/H_2O.[18] Therefore, the highly efficient degradation of pollutants came from both photoexcited AgBr and plasmon-excited Ag NPs.

Conclusions

Ag−AgBr NPs was highly dispersed on MA by the deposition−precipitation method with surfactant P123. The resulting catalyst exhibited enhanced activity and stability in the degradation of toxic persistent organic pollutants, as demonstrated with 2-CP, DCP, and TCP under visible and simulated solar light irradiation. On the basis of the studies of ESR and CV, two plasmon-induced electron-transfer process were observed from the photoexcited Ag NPs to the CB of AgBr and from 2-CP to the Ag NPs in the photoreaction system, wherein $O_2^{\bullet-}$ and excited h^+ on Ag NPs were generated by the charge separation and transfer. Also, the $^{\bullet}OH$ and $O_2^{\bullet-}$ were formed by photoexcited AgBr. Moreover, $^{\bullet}OH$ and $O_2^{\bullet-}$ radicals were primary active species, whereas the excited h^+ on Ag NPs was involved in the reaction. The high photoactivity of Ag−AgBr/MAP came from the photoexcited AgBr and plasmon-induced Ag NPs.

Acknowledgment. This work was supported by the NSFC (Nos. 20807051, 50921064, 50778169) and 863 project (No. 2006AA06Z304) and 973 project (No. 2010CB933600) and the project of the State Key Laboratory of Environmental Aquatic Chemistry (No. 08Z01ESPCR).

Supporting Information Available: Figures of cycling runs in photodegradation, photocurrent changes, and deconvoluted subbands. This material is available free of charge via the Internet at http://pubs.acs.org.

References and Notes

(1) Hoffmann, M. R.; Martin, S. T.; Choi, W.; Bahnemann, D. W. *Chem. Rev.* **1995**, *95*, 69.
(2) Martin, H. M. *Photodegradation of Water Pollutants*; CRC Press: Boca Raton, FL, 1996.
(3) Yamashita, H.; Harada, H.; Misaka, J.; Takeuchi, M.; Ikeue, K.; Anpo, M. *J. Photochem. Photobiol. A* **2002**, *148*, 257.
(4) Kontos, A. I.; Kontos, A. G.; Raptis, Y. S.; Falaras, P. *Phys. Stat. Sol. (RRL)* **2008**, *2*, 83.
(5) Khan, S. U. M.; Al-Shahry, M.; Ingler, W. B. *Science* **2002**, *297*, 2243.
(6) Sakthivel, S.; Kisch, H. *Angew. Chem., Int. Ed.* **2003**, *42*, 4908.
(7) Zou, Z.; Ye, J.; Sayama, K.; Arakawa, H. *Nature* **2001**, *414*, 625.
(8) Kim, H. G.; Hwang, D. W.; Lee, J. S. *J. Am. Chem. Soc.* **2004**, *126*, 8912.
(9) Amano, F.; Yamakata, A.; Nogami, K.; Osawa, M.; Ohtani, B. *J. Am. Chem. Soc.* **2008**, *130*, 17650.
(10) Kim, H. G.; Borse, P. H.; Choi, W.; Lee, J. S. *Angew. Chem., Int. Ed.* **2005**, *44*, 4585.
(11) Link, S.; El-Sayed, M. A. *J. Phys. Chem. B* **1999**, *103*, 8410.
(12) Jin, R.; Cao, Y. C.; Mirkin, C. A.; Kelly, K. L.; Schatzand, G. C.; Zheng, J. G. *Science* **2001**, *294*, 1901.
(13) Awazu, K.; Fujimaki, M.; Rockstuhl, C.; Tominaga, J.; Murakami, H.; Ohki, Y.; Yoshida, N.; Watanabe, T. *J. Am. Chem. Soc.* **2008**, *130*, 1676.
(14) Wang, P.; Huang, B.; Qin, X.; Zhang, X.; Dai, Y.; Wei, J.; Whangbo, M. *Angew. Chem., Int. Ed.* **2008**, *47*, 7931.
(15) Subramanian, V.; Wolf, E. E.; Kamat, P. V. *J. Am. Chem. Soc.* **2004**, *126*, 4943.
(16) Hirakawa, T.; Kamat, P. V. *J. Am. Chem. Soc.* **2005**, *127*, 3928.
(17) Hirakawa, T.; Kamat, P. V. *Langmuir* **2004**, *20*, 5645.
(18) Wang, P.; Huang, B.; Zhang, X.; Qin, X.; Hao, J.; Dai, Y.; Wang, Z.; Wei, J.; Zhan, J.; Wang, S.; Wang, J.; Whangbo, M. *Chem.—Eur. J.* **2009**, *15*, 1821.
(19) Hu, C.; Lan, Y.; Qu, J.; Hu, X.; Wang, A. *J. Phys. Chem. B* **2006**, *110*, 4066.
(20) Wang, P.; Huang, B.; Peng Wang, Qin, X.; Zhang, X.; Dai, Y.; Whangbo, M. *Inorg. Chem.* **2009**, *48*, 10697.
(21) Maldotti, A.; Molinari, A.; Amadelli, R. *Chem. Rev.* **2002**, *102*, 3811, and references therein.
(22) Xu, B.; Xiao, T.; Yan, Z.; Sun, X.; Sloan, J.; L.González-Cortés, S.; Alshahrani, F.; Green, M. L. H. *Microporous Mesoporous Mater.* **2006**, *91*, 293.
(23) Shimizu, K.; Shibata, J.; Yoshida, H.; Satsuma1, A.; Hattori, T. *Appl. Catal., B* **2001**, *30*, 151.
(24) Bethke, K. A.; Kung, H. H. *J. Catal.* **1997**, *172*, 93.
(25) Bogdanchikova, N.; Meunier, F. C.; Avalos-Borja, M.; Breen, J. P.; Pestryakov, A. *Appl. Catal., B* **2002**, *36*, 287.
(26) Li, Z.; Stephanopoulos, M. F. *J. Catal.* **1999**, *182*, 313.

JP909697K